

See discussions, stats, and author profiles for this publication at: <https://www.researchgate.net/publication/50418552>

How Does the Nickel Pincer Complex Catalyze the Conversion of CO₂ to a Methanol Derivative? A Computational Mechanistic Study

ARTICLE *in* INORGANIC CHEMISTRY · MARCH 2011

Impact Factor: 4.76 · DOI: 10.1021/ic200221a · Source: PubMed

CITATIONS

68

READS

54

5 AUTHORS, INCLUDING:



Hairong Guan

University of Cincinnati

41 PUBLICATIONS 1,492 CITATIONS

SEE PROFILE

How Does the Nickel Pincer Complex Catalyze the Conversion of CO₂ to a Methanol Derivative? A Computational Mechanistic Study

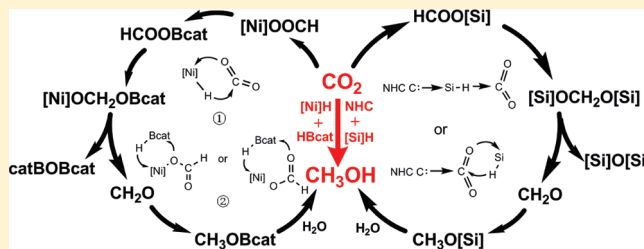
Fang Huang,[†] Chenggen Zhang,[†] Jinliang Jiang,[†] Zhi-Xiang Wang,^{*,†} and Hairong Guan^{*,‡}

[†]College of Chemistry and Chemical Engineering, Graduate University of the Chinese Academy of Sciences, Beijing, 100049, China

[‡]Department of Chemistry, University of Cincinnati, P.O. Box 21072, Cincinnati, Ohio 45221-0172, United States

Supporting Information

ABSTRACT: The mechanistic details of nickel-catalyzed reduction of CO₂ with catecholborane (HBcat) have been studied by DFT calculations. The nickel pincer hydride complex ($\{2,6\text{-C}_6\text{H}_3(\text{OP}^t\text{Bu}_2)_2\}\text{NiH} = [\text{Ni}]H$) has been shown to catalyze the sequential reduction from CO₂ to HCOOBcat, then to CH₂O, and finally to CH₃OBcat. Each process is accomplished by a two-step sequence at the nickel center: the insertion of a C=O bond into [Ni]H, followed by the reaction of the insertion product with HBcat. Calculations have predicted the difficulties of observing the possible intermediates such as [Ni]OCH₂OBcat, [Ni]OBcat, and [Ni]OCH₃, based on the low kinetic barriers and favorable thermodynamics for the decomposition of [Ni]OCH₂OBcat, as well as the reactions of [Ni]OBcat and [Ni]OCH₃ with HBcat. Compared to the uncatalyzed reactions of HBcat with CO₂, HCOOBcat, and CH₂O, the nickel hydride catalyst accelerates the H^{δ-} transfer by lowering the barriers by 30.1, 12.4, and 19.6 kcal/mol, respectively. In general, the catalytic role of the nickel hydride is similar to that of *N*-heterocyclic carbene (NHC) catalyst in the hydrosilylation of CO₂. However, the H^{δ-} transfer mechanisms used by the two catalysts are completely different. The H^{δ-} transfer catalyzed by [Ni]H can be described as hydrogen being shuttled from HBcat to nickel center and then to the C=O bond, and the catalyst changes its integrity during catalysis. In contrast, the NHC catalyst simply exerts an electronic influence to activate either the silane or CO₂, and the integrity of the catalyst remains intact throughout the catalytic cycle. The comparison between [Ni]H and Cp₂Zr(H)Cl in the stoichiometric reduction of CO₂ has suggested that ligand sterics and metal electronic properties play critical roles in controlling the outcome of the reaction. A bridging methylene diolate complex has been previously observed in the zirconium system, whereas the analogous [Ni]OCH₂O[Ni] is not a viable intermediate, both kinetically and thermodynamically. Replacing HBcat with PhSiH₃ in the nickel-catalyzed reduction of CO₂ results in a high kinetic barrier for the reaction of [Ni]OOCH with PhSiH₃. Switching silanes to HBcat in NHC-catalyzed reduction of CO₂ generates a very stable NHC adduct of HCOOBcat, which makes the release of NHC less favorable.



1. INTRODUCTION

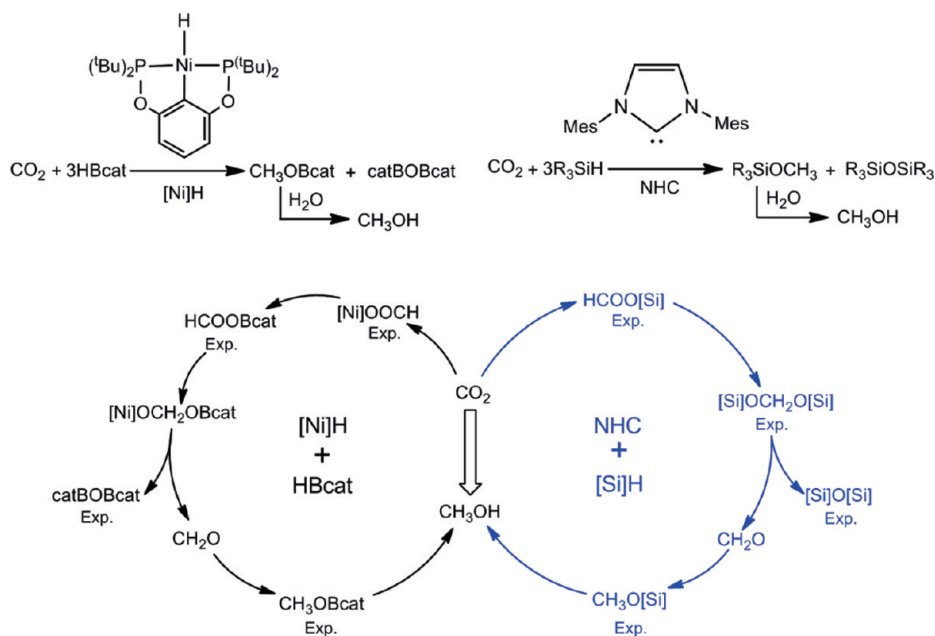
Excessive use of fossil fuels has significantly raised the CO₂ concentration in the atmosphere, which is one of the leading factors in global warming. On the other hand, CO₂ can serve as an abundant and inexpensive carbon source for the synthesis of value-added chemicals.^{1,2} Among many catalytic processes involving CO₂, its reduction to CH₄,³ CH₃OH,⁴ HCOOH,^{5–7} or CO^{8–10} promoted by homogeneous transition-metal complexes is a promising way to utilize this specific greenhouse gas. For practical applications, the conversion CO₂ to CH₃OH is particularly attractive, because of the convenience in transporting and storing a liquid fuel. Floriani and co-workers have reported that Cp₂Zr(H)Cl, which is an early-transition-metal complex, can be used to mediate the stoichiometric conversion of CO₂ to CH₃OH.^{4g,h} Sasaki and co-workers have shown a catalytic system that uses Ru₃(CO)₁₂-KI to promote the hydrogenation of CO₂ to a mixture of CH₄, CH₃OH, and CO.^{4f} Eisenschmid and Eisenberg demonstrated that Ir(CN)(CO)(dppe) [dppe = 1,

2-bis(diphenylphosphino)ethane] is a viable catalyst for the hydrosilylation of CO₂ to the methoxide level.⁴ⁱ Recently, transition-metal-free systems such as TMP/B(C₆F₅)₃/H₂ (reported by the Ashley and O'Hare groups^{4c}) and PMe₃/AlX₃/NH₃BH₃ (reported by the Stephan group^{4b}) have also been used to achieve the reduction of CO₂. Computationally, Chan and Radom have examined the strategies of using zeolite catalysts to convert CO₂ to methanol.^{4d,e}

Recently, Zhang et al. have reported organocatalytic transformation of CO₂ into CH₃OH derivatives using an *N*-heterocyclic carbene (NHC) as the catalyst and silanes (R₃SiH = [Si]H) as the reducing reagents (termed as NHC/CO₂/silane system).¹¹ One of us has reported the catalytic conversion of CO₂ to a methoxy boron compound, using a nickel pincer hydride complex ($\{2,6\text{-C}_6\text{H}_3(\text{OP}^t\text{Bu}_2)_2\}\text{NiH} = [\text{Ni}]H$) as the catalyst and catecholborane

Received: February 1, 2011

Published: March 17, 2011

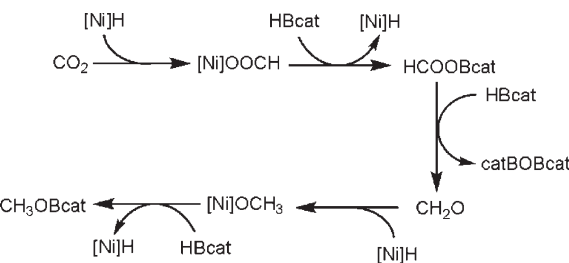
Scheme 1. Comparison between $[\text{Ni}]H$ - and NHC-Catalyzed CO_2 Reduction Reactions^a

^a “Exp.” denotes experimentally observed species.

(HBcat) as the hydrogen source (termed as the $[\text{Ni}]H/\text{CO}_2/\text{HBcat}$ system).¹² Close examination of the experimental details of these two systems, as summarized in Scheme 1, has revealed some interesting similarities. First of all, both systems use 3 equiv of hydrogen sources to reduce 1 equiv of CO_2 . Second, in terms of experimentally detected species, there are several one-to-one correlations (i.e., $\text{HCOOBcat} \leftrightarrow \text{HCOO[Si]}$, $\text{catBOBcat} \leftrightarrow [\text{Si}]O[\text{Si}]$, and $\text{CH}_3\text{OBcat} \leftrightarrow \text{CH}_3\text{O[Si]}$). In addition, CH_2O has been proposed as an important intermediate in the catalytic cycle of $[\text{Ni}]H/\text{CO}_2/\text{HBcat}$ system.¹² Our previous study of the NHC/ CO_2 /silane system has showed that CH_2O is also an inevitable intermediate,¹³ although it has not been reported in the experimental study.¹¹ There are also several differences in these two catalytic systems. For example, $[\text{Si}]O\text{CH}_2\text{O}[Si]$ has been detected in the NHC/ CO_2 /silane system, whereas $\text{catBOCH}_2\text{OBcat}$ has not been observed. While $[\text{Ni}]OOCH$ has been found in the $[\text{Ni}]H/\text{CO}_2/\text{HBcat}$ system, the counterpart in the NHC/ CO_2 /silane system remains elusive. Furthermore, unlike the NHC/ CO_2 /silane system, where the NHC catalyst has been shown to participate in three $\text{H}^{\delta-}$ transfer steps, the $[\text{Ni}]H$ catalyst has been proposed to promote two $\text{H}^{\delta-}$ transfer steps, with the second $\text{H}^{\delta-}$ transfer step ($\text{HCOOBcat} + \text{HBcat} \rightarrow \text{CH}_2\text{O} + \text{catBOBcat}$) being left uncatalyzed. To further understand these two catalytic systems, we have performed a detailed computational study to gain the mechanistic insights into Ni-catalyzed reduction of CO_2 with HBcat. We have compared the results with our previously investigated NHC/ CO_2 /silane catalytic system, as well as the stoichiometric reduction of CO_2 mediated by other transition-metal hydride complexes.

2. COMPUTATIONAL DETAILS

Calculations throughout this paper were performed on the full structures of the reported compounds, rather than their truncated models. All the structures were optimized and characterized as minima or transition states at the B3LYP¹⁴/BSI level (BSI designates the basis

Scheme 2. Proposed Mechanism for the Catalytic Conversion of CO_2 to CH_3OBcat 

set with a combination of LanL2DZ¹⁵ for Ni and 6-31G* for all nonmetal atoms) in the gas phase. At the B3LYP/BSI structures, the energies were then refined by the B3LYP/6-31+G** (i.e., 6-31+G** basis set used for all atoms, including Ni) single-point calculations with the solvation effects of toluene (experimentally used) included and simulated by IEFPCM¹⁶ solvent model. The gas-phase B3LYP/BSI frequencies were used for thermal and entropic corrections at 298.15 K and 1 atm. The free energies are discussed, unless otherwise specified, and the enthalpies are given for reference. Natural bond orbital (NBO)¹⁷ analyses were performed at the B3LYP/6-31+G** level to assign the atomic charges (Q) and to measure the Wiberg bond indices (WBI). The suitability of single-point energy refinements at the structures optimized using the relatively small BSI basis set was examined. We selected some stationary points and reoptimized them at the B3LYP/6-31+G** level. The energetic results from these optimization calculations agree with the B3LYP/6-31+G**//B3LYP/BSI values within a deviation of <0.4 kcal/mol (see section SI1 in the Supporting Information). Meanwhile, for these representative stationary points, the B3LYP/6-31+G**//B3LYP/BSI relative energies were examined in comparison with the B3LYP/6-311+G**//B3LYP/BSI values; they are in reasonable agreement with each other (see section SI1 in the Supporting Information). All the optimized structures involved in this study are given in section SI2 in the Supporting Information. In the main text, we only present the optimized

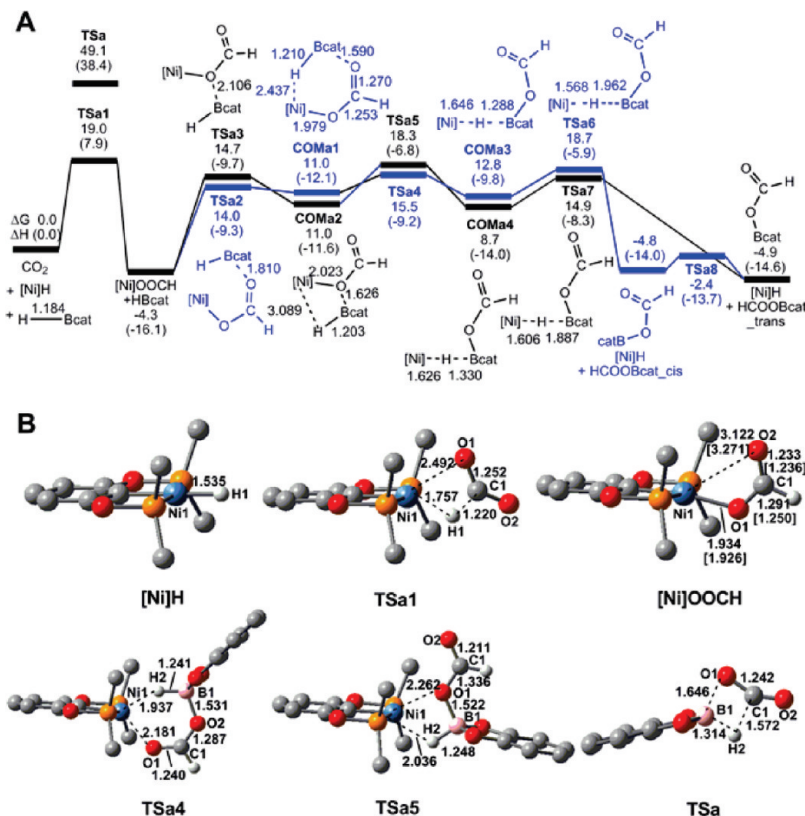


Figure 1. (A) Free-energy profile of HCOOBcat formation steps (values given in kcal/mol; the enthalpy values are listed in the parentheses). The key bond lengths in the stationary points are given in Ångstroms. (B) Optimized structures of important stationary points with key bond lengths (given in Ångstroms). Optimized structures of other stationary points are given in section SI2 in the Supporting Information. The bond lengths of [Ni]OOCH (given in the brackets) are based on X-ray data. Trivial H atoms and the methyl groups on the pincer ligand of [Ni]H are omitted for the sake of clarity.

structures of important stationary points. All calculations were carried out using Gaussian 03.¹⁸

3. RESULTS AND DISCUSSION

3.1. Overall Catalytic Mechanism. In the experimental study of the [Ni]H/CO₂/HBcat system, intermediate [Ni]OOCH and HCOOBcat were identified, along with the two products CH₃OBcat and catBOBcat.¹² A mechanism including all these species was proposed and depicted in Scheme 2. Although CH₂O was not detected experimentally, it was postulated to be generated via the reaction of HCOOBcat with HBcat. Our calculations show that CH₂O is indeed an important intermediate; however, its formation from HCOOBcat is catalyzed by [Ni]H (vide infra). In the following sections, we describe our computational results following the proposed reaction segments in Scheme 2.

Formation of HCOOBcat. Figure 1A illustrates the reaction pathways for the formation of HCOOBcat, which involves the initial CO₂ insertion into the Ni–H bond of [Ni]H via the transition state TSa1, followed by the interaction of [Ni]OOCH with 1 equiv of HBcat. The insertion of CO₂ into a metal hydride complex is often the first elemental step in transition-metal-catalyzed hydrogenation of CO₂ to HCOOH, and its mechanistic details are well understood.⁷ For a related nickel PCP-pincer system [PCP = 2,6-C₆H₃(CH₂PtBu₂)₂], Hazari et al. have studied the insertion of CO₂ into Ni–R (R = H, Me, and allyl) bonds.¹⁹ In the present case, CO₂ insertion crosses a barrier of

19.0 kcal/mol (TSa1) and is exergonic by 4.3 kcal/mol. The low barrier and small exergonicity are consistent with the experimental observation that the insertion reaction is rapid and reversible at ambient temperature. The computed enthalpy (24.0 kcal/mol) for the decarboxylation of [Ni]OOCH, the reverse step of CO₂ insertion, is also in accordance with the experimentally determined value (21.6 ± 1.1 kcal/mol).²⁰ Furthermore, the optimized structure of [Ni]OOCH is in reasonable agreement with the X-ray data (see [Ni]OOCH in Figure 1B), supporting the suitability of the employed computational method.

The insertion product [Ni]OOCH reacts with HBcat (the first equivalent of HBcat used in a complete catalytic cycle) to give the experimentally detected HCOOBcat and regenerate the [Ni]H catalyst. As shown in the schematic structures of the transition states TSa2 and TSa3, the electron-deficient B atom of HBcat attacks either of the O atoms of [Ni]OOCH via a donor–acceptor interaction, which creates two independent pathways (see Figure 1A). After crossing TSa2 or TSa3, the attack of HBcat first leads to a six-membered (COMa1) or a four-membered donor–acceptor complex (COMa2). The H^{δ-} of HBcat moiety in the complex is then transferred to the Ni center of [Ni]OOCH by crossing the transition states TSa4 or TSa5, forming a H-bridged complex (COMa3 or COMa4). The dissociation of the H-bridged complex produces HCOOBcat and regenerates the [Ni]H catalyst after crossing the transition states TSa6 or TSa7. The transition states for HCOOBcat dissociation (TSa6) and H^{δ-} transfer (TSa5) are the highest stationary points on the

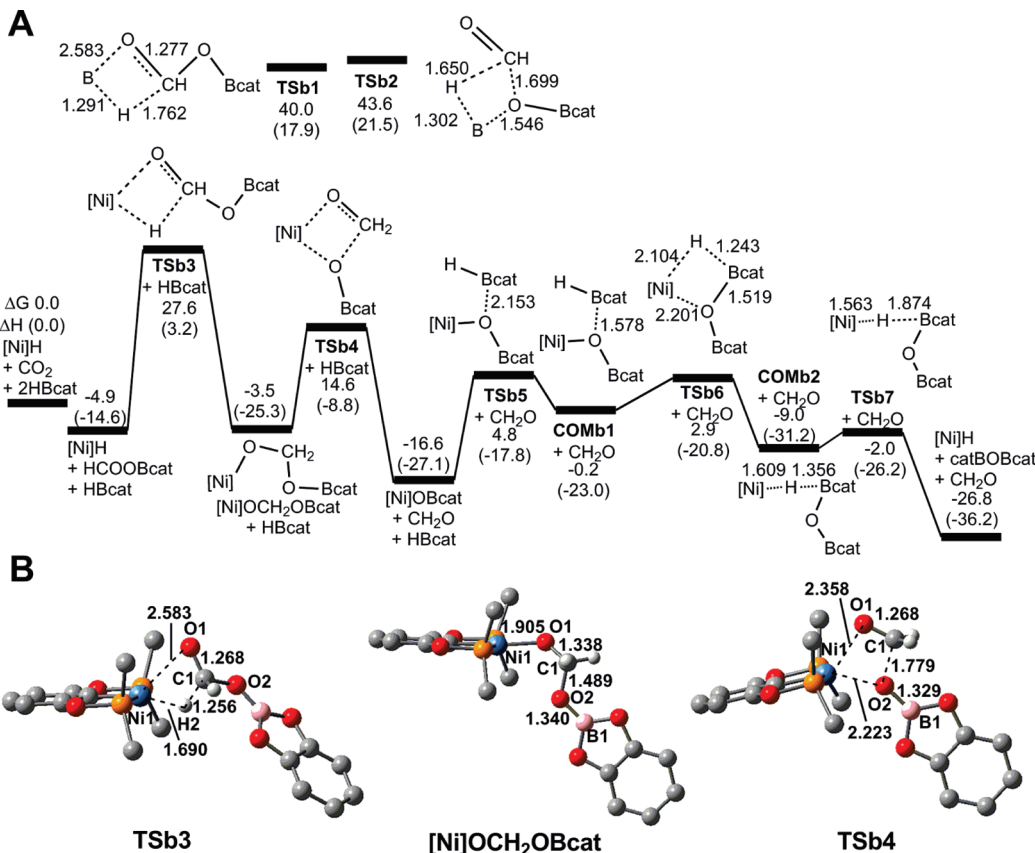


Figure 2. (A) Free-energy profile of CH₂O formation steps (values in kcal/mol; the enthalpy values are listed in the parentheses). The key bond lengths in the stationary points are given in Ångstroms. (B) Optimized structures of important stationary points with key bond lengths (given in Ångstroms). Other optimized structures are given in section S12 in the Supporting Information. Trivial H atoms and the methyl groups on the pincer ligand of [Ni]H are omitted for the sake of clarity.

two pathways (starting from [Ni]OOCH + HBcat) involving the six-membered and the four-membered donor–acceptor complex, respectively. Relative to [Ni]OOCH + HBcat, the energies of these transition states are 23.0 kcal/mol (TSa6) and 22.6 kcal/mol (TSa5). The products of either process, [Ni]H + HCOOBcat, are slightly lower than [Ni]OOCH + HBcat in free energies. These results indicate that both reaction pathways are favorable. HCOOBcat generated via TSa6 adopts a *cis* conformation (defined based on the relationship between B–O and O=C bonds), which can be easily isomerized to the *trans* conformation by only overcoming a small rotation barrier of 2.4 kcal/mol (TSa8). Because the *trans*-HCOOBcat is slightly more stable than its *cis* isomer and they are readily interconverted, we considered only the *trans*-HCOOBcat in the subsequent studies, without specifying its conformation.

Formation of CH₂O. Formaldehyde was not detected in the experiment, but it was proposed to be directly generated from the reaction between HCOOBcat and HBcat. We first examined the direct reaction and considered two possible pathways. The transition states TSb1 and TSb2 (shown in Figure 2A) correspond to the attack of HBcat on the C=O double bond and C–O single bond of HCOOBcat, respectively. While TSb2 leads to CH₂O directly, TSb1 gives catBOCH₂OBcat, which undergoes decomposition to generate CH₂O and catBOBcat. Nevertheless, the predicted barriers of 40.0 kcal/mol (via TSb1) and 43.6 kcal/mol (via TSb2), relative to 2HBcat + CO₂, are too high to be accessible experimentally at ambient temperature.

Therefore, we suspected that [Ni]H might catalyze the formation of CH₂O.

The pathway of [Ni]H-catalyzed formation of CH₂O is shown in Figure 2A. The [Ni]H complex reacts with HCOOBcat, resulting in [Ni]OCH₂OBcat, which is decomposed to [Ni]OBcat and CH₂O. The regeneration of [Ni]H is accomplished via the reaction of [Ni]OBcat with HBcat (the second equivalent of HBcat used in a complete catalytic cycle). Analogous to the direct reaction of HCOOBcat with HBcat, as indicated in TSb1 and TSb2, [Ni]H can possibly approach either the C=O or C–O single bond of HCOOBcat. However, the attack on the C–O single bond is highly unlikely, because of the steric clash between HCOOBcat and the bulky ^tBu groups of [Ni]H. Moreover, even in a less sterically crowded situation (see the top of Figure 2A), the interaction between the H–B bond and the C=O double bond (via TSb1) is more favorable than the alternative pathway (via TSb2) by 3.6 kcal/mol. Therefore, we only need to consider the attack of [Ni]H on the C=O double bond of HCOOBcat. The barrier (TSb3) for this step is 32.5 kcal/mol, with respect to [Ni]H + HCOOBcat. The value is substantially lower than that of an uncatalyzed process through either TSb1 (40.0 kcal/mol) or TSb2 (43.6 kcal/mol), suggesting the necessity of involving [Ni]H.

The intermediate [Ni]OCH₂OBcat is decomposed to CH₂O and [Ni]OBcat and the decomposition barrier (TSb4) of 18.1 kcal/mol is small enough to be experimentally reachable. One of the decomposition products [Ni]OBcat further reacts with HBcat to

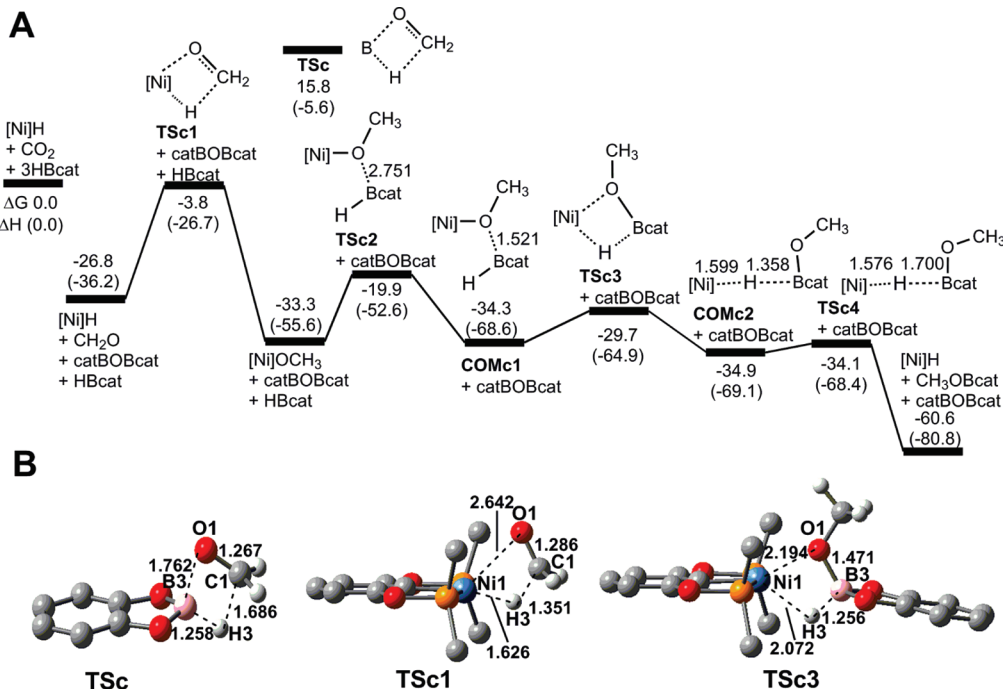


Figure 3. (A) Free-energy profile for CH_3OBcat formation steps (values in kcal/mol; the enthalpy values are listed in the parentheses). The key bond lengths labeled in the stationary points are given in Ångströms. (B) Optimized structures of important stationary points with key bond lengths (given in Ångströms). Other optimized structures are given in section SI2 in the Supporting Information. Trivial H atoms and the methyl groups on the pincer ligand of $[\text{Ni}] \text{H}$ are omitted for the sake of clarity.

reform the $[\text{Ni}] \text{H}$ catalyst. The reaction of $[\text{Ni}] \text{OBcat}$ with HBcat gives a donor–acceptor complex **COMb1** after crossing the transition state **TSb5** ($\Delta G^\ddagger = 21.4$ kcal/mol, relative to $\text{HBcat} + [\text{Ni}] \text{OBcat}$). Following another transition state **TSb6**, the H^- of HBcat is transferred to the Ni center with the concurrent cleavage of the Ni–O bond of $[\text{Ni}] \text{OBcat}$. The barrier for H^- transfer is merely 3.1 kcal/mol, relative to **COMb1**. The resulting H-bridged complex **COMb2** undergoes dissociation to give $[\text{Ni}] \text{H}$ and catBOBcat , crossing a small barrier of 7.0 kcal/mol (via **TSb7**). The borate ester catBOBcat is one of two final products of the overall catalytic reaction.

Up to this point, the highest stationary point (**TSb3**) for the reduction process is 27.6 kcal/mol higher than that of the reactants ($[\text{Ni}] \text{H} + \text{CO}_2 + \text{HBcat}$). Compared to the ambient conditions used in the experiment, this value is somewhat high. However, it should be noted that the ideal gas phase model inevitably overestimates the entropic contribution for a reaction in a solvent medium.²¹ Accurate prediction of enthalpies and entropies in solution remains a challenge for computational chemists and no standard approach is currently available.²² Nevertheless, in a study of the solvation free energy of aqueous ferric ion, Martin et al.^{23a} have proposed to correct the overestimation of entropic contributions by artificially elevating the reaction pressure from 1 atm to 1354 atm. This method was then extended to the studies of the solvation free energies of heavy transition-metal ions.^{23b,c} According to the approach, a free-energy correction of 4.3 kcal/mol is applied to the per component change for a reaction at 298.15 K and 1 atm (i.e., a reaction from *m*- to *n*-components has a free-energy correction of $(n - m) \times 4.3$ kcal/mol). If such a correction is employed, the barrier to **TSb3** is 19.0 kcal/mol higher than that of $[\text{Ni}] \text{H} + \text{CO}_2 + \text{HBcat}$ in free energy, which is in agreement with the ambient experimental conditions for the catalytic conversion.

The mechanism for CH_2O production (Figure 2A) is quite similar to what has been predicted in the NHC/ CO_2 /silane system. The $[\text{Si}] \text{OCH}_2\text{O}[\text{Si}]$ species in NHC/ CO_2 /silane system is related to $[\text{Ni}] \text{OCH}_2\text{OBcat}$ in the current system. Although $[\text{Ni}] \text{OCH}_2\text{OBcat}$ was not experimentally detected, its formation from $[\text{Ni}] \text{H}$ and HCOOBcat is demonstrated here to be energetically feasible. In addition, there are several precedents in the literature for related transition-metal complexes. For instance, Berger et al. have provided spectroscopic evidence of $[\text{Zr}] \text{OCH}_2\text{O}[\text{Zr}]$ in the stoichiometric reaction of $\text{Cp}_2\text{Zr}(\text{H})\text{Cl}$ ($[\text{Zr}] \text{H}$) with CO_2 .²⁴ Rankin and Cummins have also detected $[\text{Ta}] \text{OCH}_2\text{O}[\text{Ta}]$ in their recent investigation of the stoichiometric reaction between $(\text{Ar}[\text{tBuCH}_2]\text{N})_2(\eta^2\text{-tBu(H)-CNar})\text{TaH}$ ($[\text{Ta}] \text{H}$) and CO_2 .^{2c} The proposed $[\text{Ni}] \text{OCH}_2\text{OBcat}$ species in the nickel pincer system is probably converted so rapidly to CH_2O and $[\text{Ni}] \text{OBcat}$ that it cannot be directly observed with common spectroscopic methods. In contrast, the $[\text{Si}] \text{OCH}_2\text{O}[\text{Si}]$ species in the NHC/ CO_2 /silane system was captured by GC-MS.¹¹ The difference between these two systems is due to the kinetic barriers for the decomposition of the bridging methylene diolate complexes. The calculated barrier for $[\text{Si}] \text{OCH}_2\text{O}[\text{Si}]$ decomposition (26.2 kcal/mol) is 8.1 kcal/mol higher than the barrier for $[\text{Ni}] \text{OCH}_2\text{OBcat}$ decomposition. This result confirms that $[\text{Ni}] \text{OCH}_2\text{OBcat}$ is much less persistent than $[\text{Si}] \text{OCH}_2\text{O}[\text{Si}]$ in the NHC/ CO_2 /silane system. Similarly, intermediate $[\text{Ni}] \text{OBcat}$ in Figure 2A is also short-lived, as the barrier for the reaction of $[\text{Ni}] \text{OBcat}$ with HBcat is relatively low (21.4 kcal/mol via **TSb5**). Furthermore, the decomposition of $[\text{Ni}] \text{OCH}_2\text{OBcat}$ and the reaction of $[\text{Ni}] \text{OBcat}$ with HBcat are exoergic by 13.1 and 10.2 kcal/mol, which provide the thermodynamic sink and contribute to the difficulty of detecting these species.

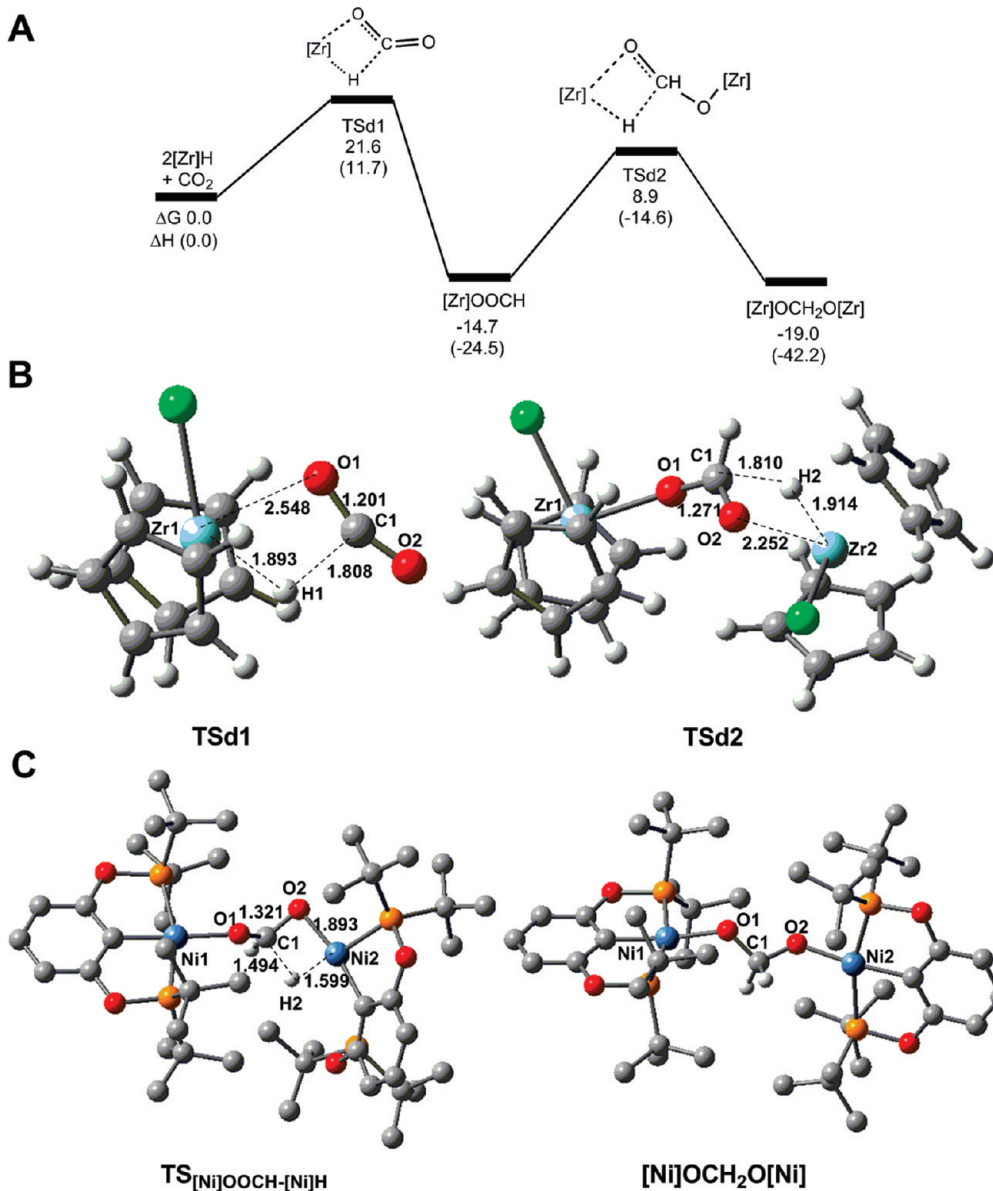


Figure 4. (A) Free-energy profile of the $[\text{Zr}]H/\text{CO}_2$ system (values in kcal/mol; enthalpy values are listed in the parentheses). (B) Optimized structures of important stationary points in the $[\text{Zr}]H/\text{CO}_2$ system with key bond lengths (given in Ångströms). Other optimized structures are given in section SII in the Supporting Information. (C) Optimized structures of the transition state (left) and the product (right) for the reaction of $[\text{Ni}]OOCH$ with $[\text{Ni}]H$. Trivial H atoms on the pincer ligand of $[\text{Ni}]H$ are omitted for the sake of clarity.

Formation of CH_3OBcat . CH_3OBcat is the other final product of CO_2 reduction. As shown in Figure 3A, the formation of CH_3OBcat starts with the insertion of CH_2O into the $\text{Ni}-\text{H}$ bond, which is similar to CO_2 and HCOOBcat insertions (see Figure 1A and 2A). The reaction of CH_2O overcomes the transition state $\text{TS}\text{c1}$ ($\Delta G^\ddagger = 23.0$ kcal/mol) to afford $[\text{Ni}]\text{OCH}_3$. The latter species interacts with HBcat (the third equivalent of HBcat used in a complete catalytic cycle) to give the donor–acceptor complex COMc1 after crossing the barrier over $\text{TS}\text{c2}$ ($\Delta G^\ddagger = 13.4$ kcal/mol). The four-membered transition state $\text{TS}\text{c3}$ (4.6 kcal/mol) results in the transfer of $\text{H}^\delta-$ from HBcat to the Ni center of $[\text{Ni}]\text{OCH}_3$, providing the H -bridged complex COMc2 . The dissociation of this complex gives CH_3OBcat and the $[\text{Ni}]H$ catalyst by passing a very low barrier of 0.8 kcal/mol (via $\text{TS}\text{c4}$). The energy profile in Figure 3A suggests that the reduction of CH_2O

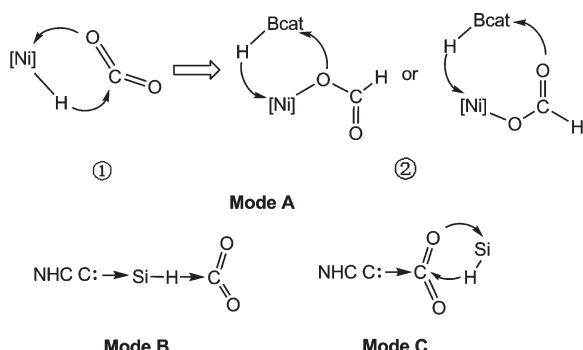
is energetically favorable; the highest barrier ($\text{TS}\text{c1}$) in the entire process is 23.0 kcal/mol. Because of the low barrier (13.4 kcal/mol) for the reaction of $[\text{Ni}]\text{OCH}_3$ with HBcat , the direct observation of $[\text{Ni}]\text{OCH}_3$ is expected to be challenging. The above-mentioned hydroboration of CH_2O promoted by $[\text{Ni}]H$ has been indirectly tested by experiments.¹² To avoid the complication of water in commercially available formaldehyde solution, paraformaldehyde was used instead as the substrate to react with $[\text{Ni}]H$. The insertion reaction was sluggish at room temperature, limited by the slow release of CH_2O from paraformaldehyde. Once the nickel alkoxide was formed, its subsequent reaction with HBcat proved to be fast at room temperature.

3.2. Catalytic Effect of $[\text{Ni}]H$. The computational studies show that each of the three reaction segments involves the transfer of $\text{H}^\delta-$ from $[\text{Ni}]H$ to the carbon atom of CO_2 ,

HCOOBcat, or CH₂O via an insertion reaction (see **TSa1**, **TSb3**, and **TSc1**). Alternatively, HBcat is capable of transferring H^{δ−} directly to these compounds. To understand the catalytic effect of [Ni]H, the uncatalyzed reactions of HBcat with CO₂, HCOOBcat, and CH₂O were also studied. As compared in Figures 1A–3A, the H^{δ−} transfer from [Ni]H complex is much more favorable than the direct H^{δ−} transfer from HBcat; **TSa1**, **TSb3**, and **TSc1** are 30.1, 12.4, and 19.6 kcal/mol lower than **TSa** (Figure 1A), **TSb1** (Figure 2A), and **TSc** (Figure 3A), respectively. The more facile H^{δ−} transfer from [Ni]H reflects the more-negative H^{δ−} of the Ni–H bond ($Q = -0.135\text{ e}$) than that of the B–H bond in HBcat ($Q = -0.076\text{ e}$) and the weaker Ni–H bond (WBI = 0.680) than B–H bond (WBI = 0.970).

It has been reported that the reaction of Cp₂Zr(H)Cl ([Zr]H) with CO₂ yields [Zr]OCH₂O[Zr] (and eventual [Zr]OCH₃)^{4g,h,24} and the reaction of (Ar[^tBuCH₂]N)₂(η^2 -^tBu(H)CNAr)TaH ([Ta]H) complex with CO₂ leads to [Ta]OCH₂O[Ta].^{2c} In principle, a stoichiometric reaction of [Ni]H with CO₂ could also give rise to a complex with CH₂O bridging two nickel centers. Such a species may play an important role in the [Ni]H/CO₂/HBcat catalytic cycle. However, this dinickel species was never observed experimentally. This prompted us to ask the following question: What makes these metal hydride systems so different in the reactivity? Using the reaction of [Zr]H with CO₂ as a representative example, we studied the free-energy profile (Figure 4A) assuming that the reaction goes through an intermediate [Zr]OOCH (similar to [Ni]OOCH in Figure 1A).²⁵ Interestingly, neither the barrier for CO₂ insertion (21.6 kcal/mol) nor the barrier for the reaction of [Zr]OOCH with [Zr]H (23.6 kcal/mol) is high. The dizirconium species [Zr]OCH₂O[Zr] is 19.0 kcal/mol lower than CO₂ + 2[Zr]H. In strong contrast, the reaction [Ni]OOCH + [Ni]H → [Ni]OCH₂O[Ni] is extremely unfavorable, both kinetically and thermodynamically; the barrier for the reaction is 62.7 kcal/mol and the reaction is endoergic by 42.8 kcal/mol. Consistent with the calculations, when equimolar amounts of [Ni]H and [Ni]OOCH were mixed in toluene at room temperature or 60 °C, no new species was observed.²⁰ The significant reactivity difference between [Ni]H and [Zr]H can be attributed to both steric and electronic effects. As demonstrated by the optimized structures in Figure 4C, there is severe steric repulsion between two approaching nickel pincer complexes. In the transition state, one of the P^tBu₂ arms must dissociate from the nickel center. In addition, the higher oxyphilicity of the early transition metals (i.e., Zr) may contribute to their unique reaction patterns. In an attempt to separate the steric effect from the overall effects, we replaced the four ^tBu groups in [Ni]H with four Me groups in our calculations. The new [Ni]OCH₂O[Ni] is still 26.9 kcal/mol higher in energy than its corresponding reactants; however, this value is significantly less than 42.8 kcal/mol, corresponding to the original [Ni]OCH₂O[Ni]. While [Ni]H does not react with [Ni]OOCH, HBcat is able to react with the [Ni]OOCH, thereby completing the catalytic transformation according to the pathways predicted in Figures 1A–3A. [Zr]H and [Ta]H hydride complexes have the proper and electronic structures to allow them to react with [Zr]OOCH and [Ta]OOCH to give complex [Zr]OCH₂O[Zr] and [Ta]OCH₂O[Ta], respectively. However, breaking the strong Zr–O and Ta–O bonds is expected to be too difficult to close a potential catalytic cycle. Finally, the M06 method,^{26,27} which gives a better description of noncovalent interactions than B3LYP method, was employed to further study the reaction [Ni]OOCH + [Ni]H → [Ni]OCH₂O[Ni]. The high barrier (45.8 kcal/mol) and endogoncity (42.8 kcal/mol) once again verify the difficulty of the reaction.

Scheme 3. The H^{δ−} Transfer Mechanism with [Ni]H (Mode A) and Direct H^{δ−} Transfer Mechanism with NHC (Modes B and C)^a



^a Segments ① and ② are described in the text.

3.3. Catalytic Roles of [Ni]H and NHC: Similarities and Differences. The NHC/CO₂/silane and [Ni]H/CO₂/HBcat systems are prototypical examples of CO₂ reduction catalyzed by organic compounds and transition-metal complexes, respectively. For the deeper understanding of this important transformation, it is imperative to compare the roles of the two catalytic systems. Both systems feature three H^{δ−} transfer steps; therefore, 3 equiv of hydrogen sources are needed to reduce 1 equiv of CO₂. The overall function of the catalysts is to facilitate the transfer of H^{δ−} from the hydrogen source (HBcat or silane) to CO₂/HCOOBcat/CH₂O in the [Ni]H/CO₂/HBcat system or to CO₂/HCOO[Si]/CH₂O in the NHC/CO₂/silane system. How the two catalysts promote the H^{δ−} transfer is, however, completely different. We use the first H^{δ−} transfer step as an example to illustrate the differences. In the [Ni]H case, H^{δ−} transfer is achieved through two sequential steps (Mode A in Scheme 3): in ①, the [Ni]H catalyst first transfers its own H^{δ−} to CO₂ to generate [Ni]OOCH, and in ②, the nickel complex receives H^{δ−} from HBcat to reform [Ni]H and release HCOOBcat. The integrity of the catalyst structure changes during catalysis (see Figures 1A–3A). In comparison, the NHC catalyst either activates the silane via Mode B or facilitates the direct H^{δ−} transfer from silane to an activated CO₂ via Mode C (Scheme 3). In the H^{δ−} transfer process, the NHC catalyst simply exerts electronic influence to promote the reaction but never gains or loses an H atom. In other words, the integrity of the NHC catalyst structure never changes during catalysis. As a result of direct H^{δ−} transfer from the silane, there are no intermediates that are equivalent to [Ni]OOCH, [Ni]OCH₂OBcat, and [Ni]OCH₃ in the NHC/CO₂/silane system. This also explains that, in the NHC/CO₂/silane system, the intermediate after the second H^{δ−} transfer step is [Si]OCH₂O[Si], with no involvement of the catalyst. In the [Ni]H/CO₂/HBcat system, the intermediate after the second H^{δ−} transfer step is [Ni]OCH₂OBcat with nickel catalyst incorporated, rather than catBOCH₂OBcat, as one might have imagined. The experimentally detected species including HCOOBcat, catBOBcat, and CH₃OBcat are generated from the corresponding nickel species ([Ni]OOCH, [Ni]OBcat, and [Ni]OCH₃) and HBcat; they also correlate to the observed HCOO[Si], [Si]O[Si], and CH₃O[Si] in the NHC/CO₂/silane system.

Both catalytic systems use an external hydrogen source to provide H^{δ−}. We were curious to see if the hydrogen sources of the two systems can be switched. To answer this question, we considered the energetics of the first H^{δ−} transfer step in the two

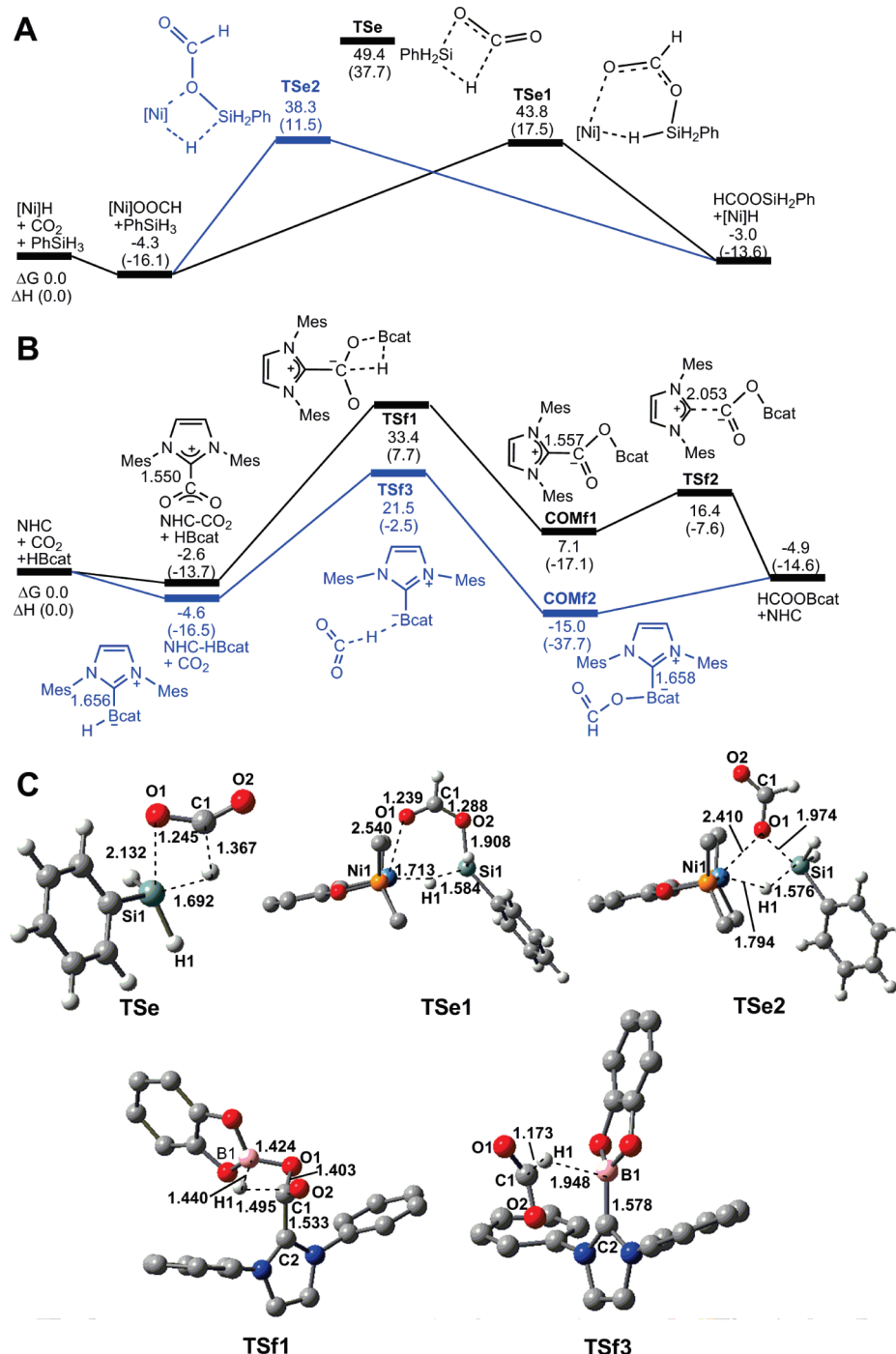


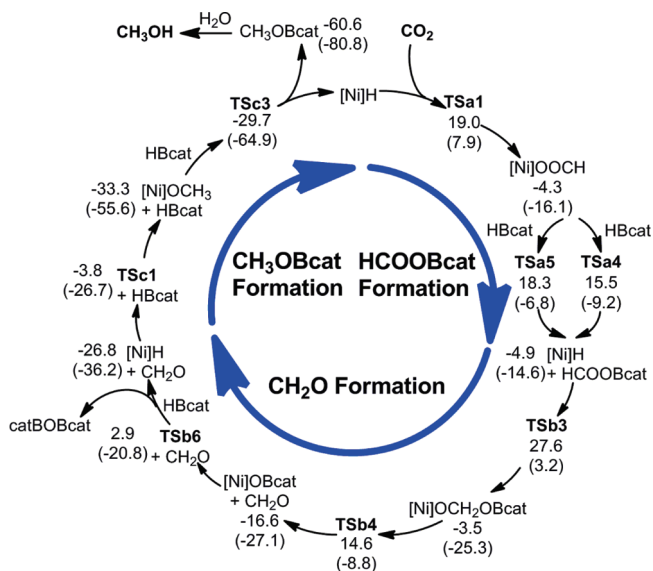
Figure 5. Free-energy profiles of (A) the $[Ni]H/CO_2/PhSiH_3$ system and (B) the $NHC/CO_2/HBcat$ system. (Values are given in kcal/mol; the enthalpy values are listed in parentheses. The key bond lengths in the stationary points are given in Ångströms.) (C) Optimized structures of important stationary points with key bond lengths (values shown in black, given in Ångströms). Other optimized structures are given in section SI2 in the Supporting Information. Trivial H atoms, the methyl groups on the pincer ligand of $[Ni]H$, and the methyl groups on the mesityl rings of NHC are omitted for the sake of clarity.

systems termed as $[Ni]H/CO_2/PhSiH_3$ and $NHC/CO_2/HBcat$. The results are summarized in Figure 5.

Without the participation of $[Ni]H$, the direct reaction of $PhSiH_3$ with CO_2 has a barrier of 49.4 kcal/mol (via TSe), which is about the same as that over TSa ($\Delta G^\ddagger = 49.1$ kcal/mol; see Figure 1) for the direct reaction of $HBcat$ with CO_2 . The small difference in these barriers implies that $PhSiH_3$ and $HBcat$ have comparable $H^{\delta-}$ donor ability. However, the catalytic influence

of $[Ni]H$ in $[Ni]H/CO_2/PhSiH_3$ system is not as effective as that in the $[Ni]H/CO_2/HBcat$ system. The relative energies of the six-membered and four-membered transition states (48.1 kcal/mol for $TSe1$ and 42.6 kcal/mol for $TSe2$) are much higher than the values of the corresponding transition states in the $[Ni]H/CO_2/HBcat$ system (19.8 kcal/mol for $TSa4$ and 22.6 kcal/mol for $TSa5$). The energetic differences can be rationalized by comparing the chemical bonding in the transition states. The

Scheme 4. A Complete Catalytic Cycle of [Ni]H-Catalyzed Reduction of CO₂ to CH₃OBcat^a



^a For the sake of clarity, trivial stationary points are not included.

formation of the O₂—Si1 (TSe1) or O₁—Si1 (in TSe2) bond distorts the tetrahedral geometry at the Si center and results in a pentacoordinated Si center, which pays a significantly high reorganization energy.²⁸ In contrast, the O₂ atom in TSa4 or the O₁ atom in TSa5 interacts favorably with an electron-deficient B atom via a donor–acceptor interaction. Note that the barriers for other silanes may vary greatly; however, the general conclusion that silanes are not as good as HBcat to serve as the hydrogen sources in [Ni]H-catalyzed CO₂ reduction holds true. Indeed, no reaction was observed when [Ni]OOCH was mixed with 1 equiv of PhSiH₃ at room temperature for one day.²⁰ Attempted catalytic hydrosilylation of CO₂ with PhSiH₃ in the presence of 1 mol % of [Ni]H did not yield any reduction products.

In the NHC/CO₂/HBcat system, the two barriers (33.4 kcal/mol for TSf1 and 21.5 kcal/mol for TSf3) of H^{δ−} transfer via the two different activation modes (Modes C and B in Scheme 3) are not high for experimental realization. However, the liberation of NHC catalyst in the mode B activation pathway can be problematic, because COMf2 is too stable (10.1 kcal/mol more stable than HCOOBcat + NHC). Our previous study of the NHC/CO₂/silane system has shown that NHC is very easily released and the intermediate analogous to COMf2 is even less stable than NHC + HCOO[Si]. Therefore, HBcat may not be a good hydrogen source for NHC-catalyzed CO₂ reduction. Note that the problem of releasing NHC could be circumvented through the use of a sterically more demanding NHC. Further experiments are needed to test this hypothesis.

4. CONCLUSIONS

Our computational mechanistic study has elucidated how [Ni]H facilitates the catalytic conversion of CO₂ to a methanol derivative. As shown in the complete catalytic cycle (Scheme 4), the overall transformation involves three H^{δ−} transfer steps and [Ni]H participates in each one of them. The catalytic role of [Ni]H is to shuttle H^{δ−} from HBcat to CO₂, HCOOBcat, and

CH₂O. The direct reaction of HBcat with CO₂ is highly unfavorable. The predicted intermediates [Ni]OCH₂OBcat, [Ni]OBcat, and [Ni]OCH₃ could be fleeting species, because of the facile decomposition of [Ni]OCH₂OBcat and low barriers for the reactions of [Ni]OBcat and [Ni]OCH₃ with HBcat. In comparison, the NHC catalyst in the NHC/CO₂/silane system facilitates the direct H^{δ−} transfer from silane to CO₂, HCOO[Si], and CH₂O. The integrity of the catalyst structure never changes during the entire process. Switching the hydrogen sources in the two catalytic systems results in less-favorable reactions. The [Ni]H/CO₂/PhSiH₃ system has a high kinetic barrier for the reaction between [Ni]OOCH and PhSiH₃, while the NHC/CO₂/HBcat system has a thermodynamically stable intermediate (NHC-HCOOBcat) that makes the release of NHC problematic. The present study has demonstrated that, depending on the reaction mechanism, the CO₂ reduction catalyst should be matched with an appropriate hydrogen source.

■ ASSOCIATED CONTENT

S Supporting Information. This material is available free of charge via the Internet at <http://pubs.acs.org>.

■ AUTHOR INFORMATION

Corresponding Author

*E-mails: zxwang@gucas.ac.cn (Z.-X.W.), hairong.guan@uc.edu (H.G.).

■ ACKNOWLEDGMENT

This work is financially supported by funds from the Chinese Academy of Sciences, the National Natural Science Foundation of China (Nos. 20973197 and 20773160, to Z.-X.W.), and the U.S. National Science Foundation (No. CHE-0952083, to H.G.).

■ REFERENCES

- (1) For recent reviews on CO₂ transformation, see: (a) Kember, M. R.; Buchard, A.; Williams, C. K. *Chem. Commun.* **2011**, 47, 141. (b) Daresbourg, D. J. *Inorg. Chem.* **2010**, 49, 10765. (c) Riduan, S. N.; Zhang, Y. *Dalton Trans.* **2010**, 39, 3347. (d) Mikkelsen, M.; Jørgensen, M.; Krebs, F. C. *Energy Environ. Sci.* **2010**, 3, 43. (e) Sakakura, T.; Kohno, K. *Chem. Commun.* **2009**, 1312. (f) Olah, G. A.; Goepert, A.; Prakash, G. K. S. *J. Org. Chem.* **2009**, 74, 487. (g) Correa, A.; Martín, R. *Angew. Chem., Int. Ed.* **2009**, 48, 6201. (h) Yu, K. M. K.; Curcic, I.; Gabriel, J.; Tsang, S. C. E. *ChemSusChem* **2008**, 1, 893. (i) Sakakura, T.; Choi, J.-C.; Yasuda, H. *Chem. Rev.* **2007**, 107, 2365. (j) Daresbourg, D. J. *Chem. Rev.* **2007**, 107, 2388. (k) Aresta, M.; Dibenedetto, A. *Dalton Trans.* **2007**, 2975. (l) Olah, G. A. *Angew. Chem., Int. Ed.* **2005**, 44, 2636. (m) Coates, G. W.; Moore, D. R. *Angew. Chem., Int. Ed.* **2004**, 43, 6618.
- (2) For recent reports on CO₂ fixation, see: (a) Buchard, A.; Kember, M. R.; Sandeman, K. G.; Williams, C. K. *Chem. Commun.* **2011**, 47, 212. (b) Ren, W.-M.; Zhang, X.; Liu, Y.; Li, J.-F.; Wang, H.; Lu, X.-B. *Macromolecules* **2010**, 43, 1396. (c) Rankin, M. A.; Cummins, C. C. *J. Am. Chem. Soc.* **2010**, 132, 10021. (d) Langer, J.; Imhof, W.; Fabra, M. J.; García-Orduña, P.; Görts, H.; Lahoz, F. J.; Oro, L. A.; Westerhausen, M. *Organometallics* **2010**, 29, 1642. (e) Kember, M. R.; White, A. J. P.; Williams, C. K. *Macromolecules* **2010**, 43, 2291. (f) He, C.; Tian, G.; Liu, Z.; Feng, S. *Org. Lett.* **2010**, 12, 649. (g) Decortes, A.; Belmonte, M. M.; Benet-Buchholz, J.; Kleij, A. W. *Chem. Commun.* **2010**, 46, 4580. (h) Clegg, W.; Harrington, R. W.; North, M.; Pasquale, R. *Chem.—Eur. J.* **2010**, 16, 6828. (i) Mömeling, C. M.; Otten, E.; Kehr, G.; Fröhlich, R.; Grimme, S.; Stephan, D. W.; Erker, G. *Angew. Chem., Int. Ed.* **2009**, 48, 6643. (j) Kember, M. R.; White, A. J. P.; Williams, C. K.

- Inorg. Chem.* **2009**, *48*, 9535. (k) Kember, M. R.; Knight, P. D.; Reung, P. T. R.; Williams, C. K. *Angew. Chem., Int. Ed.* **2009**, *48*, 931. (l) Kayaki, Y.; Yamamoto, M.; Ikariya, T. *Angew. Chem., Int. Ed.* **2009**, *48*, 4194. (m) Dang, L.; Lin, Z.; Marder, T. B. *Organometallics* **2010**, *29*, 917. (n) Li, J.; Jia, G.; Lin, Z. *Organometallics* **2008**, *27*, 3892.
- (3) (a) Berkefeld, A.; Piers, W. E.; Parvez, M. *J. Am. Chem. Soc.* **2010**, *132*, 10660. (b) Matsuo, T.; Kawaguchi, H. *J. Am. Chem. Soc.* **2006**, *128*, 12362.
- (4) (a) Roy, L.; Zimmerman, P. M.; Paul, A. *Chem.—Eur. J.* **2011**, *17*, 435. (b) Ménard, G.; Stephan, D. W. *J. Am. Chem. Soc.* **2010**, *132*, 1796. (c) Ashley, A. E.; Thompson, A. L.; O'Hare, D. *Angew. Chem., Int. Ed.* **2009**, *48*, 9839. (d) Chan, B.; Radom, L. *J. Am. Chem. Soc.* **2008**, *130*, 9790. (e) Chan, B.; Radom, L. *J. Am. Chem. Soc.* **2006**, *128*, 5322. (f) Tominaga, K.; Sasaki, Y.; Kawai, M.; Watanabe, T.; Saito, M. *J. Chem. Soc.—Chem. Commun.* **1993**, 629. (g) Gambarotta, S.; Strologo, S.; Floriani, C.; Chiesi-Villa, A.; Guastini, C. *J. Am. Chem. Soc.* **1985**, *107*, 6278. (h) Fachinetti, G.; Floriani, C.; Roselli, A.; Pucci, S. *J. Chem. Soc.—Chem. Commun.* **1978**, 269. (i) Eisenschmid, T. C.; Eisenberg, R. *Organometallics* **1989**, *8*, 1822.
- (5) For representative reviews on the conversion of CO₂ to HCOOH, see: (a) Jessop, P. G.; Joó, F.; Tai, C. C. *Coord. Chem. Rev.* **2004**, *248*, 2425. (b) Leitner, W. *Angew. Chem., Int. Ed.* **1995**, *34*, 2207. (c) Jessop, P. G.; Ikariya, T.; Noyori, R. *Chem. Rev.* **1995**, *95*, 259.
- (6) For recent experimental studies on the conversion of CO₂ to HCOOH, see: (a) Sanz, S.; Benítez, M.; Peris, E. *Organometallics* **2010**, *29*, 275. (b) Federsel, C.; Jackstell, R.; Beller, M. *Angew. Chem., Int. Ed.* **2010**, *49*, 6254. (c) Federsel, C.; Boddien, A.; Jackstell, R.; Jennerjahn, R.; Dyson, P. J.; Scopelliti, R.; Laurenczy, G.; Beller, M. *Angew. Chem., Int. Ed.* **2010**, *49*, 9777. (d) Zhang, Z.; Hu, S.; Song, J.; Li, W.; Yang, G.; Han, B. *ChemSusChem* **2009**, *2*, 234. (e) Tanaka, R.; Yamashita, M.; Nozaki, K. *J. Am. Chem. Soc.* **2009**, *131*, 14168. (f) Zhang, Z.; Xie, Y.; Li, W.; Hu, S.; Song, J.; Jiang, T.; Han, B. *Angew. Chem., Int. Ed.* **2008**, *47*, 1127. (g) Himeda, Y. *Eur. J. Inorg. Chem.* **2007**, 3927.
- (7) For recent theoretical studies on the conversion of CO₂ to HCOOH, see: (a) Ahlquist, M. S. G. *J. Mol. Catal. A-Chem.* **2010**, *324*, 3. (b) Getty, A. D.; Tai, C. -C.; Linehan, J. C.; Jessop, P. G.; Olmstead, M. M.; Rheingold, A. L. *Organometallics* **2009**, *28*, 5466. (c) Urakawa, A.; Jutz, F.; Laurenczy, G.; Baiker, A. *Chem.—Eur. J.* **2007**, *13*, 3886. (d) Huang, K. -W.; Han, J. H.; Musgrave, C. B.; Fujita, E. *Organometallics* **2007**, *26*, 508. (e) Ohnishi, Y.; Nakao, Y.; Sato, H.; Sakaki, S. *Organometallics* **2006**, *25*, 3352. (f) Ogo, S.; Kabe, R.; Hayashi, H.; Harada, R.; Fukuzumi, S. *Dalton Trans.* **2006**, 4657. (g) Ohnishi, Y.; Matsunaga, T.; Nakao, Y.; Sato, H.; Sakaki, S. *J. Am. Chem. Soc.* **2005**, *127*, 4021.
- (8) For experimental studies on CO₂ cleavage, see: (a) Silvia, J. S.; Cummins, C. C. *J. Am. Chem. Soc.* **2010**, *132*, 2169. (b) Gu, L.; Zhang, Y. *J. Am. Chem. Soc.* **2010**, *132*, 914. (c) van der Boom, M. E. *Angew. Chem., Int. Ed.* **2009**, *48*, 28. (d) Whited, M. T.; Grubbs, R. H. *J. Am. Chem. Soc.* **2008**, *130*, 5874. (e) Sadique, A. R.; Brennessel, W. W.; Holland, P. L. *Inorg. Chem.* **2008**, *47*, 784. (f) Allen, O. R.; Dalgarno, S. J.; Field, L. D. *Organometallics* **2008**, *27*, 3328. (g) Laitar, D. S.; Müller, P.; Sadighi, J. P. *J. Am. Chem. Soc.* **2005**, *127*, 17196.
- (9) For theoretical studies on CO₂ cleavage, see: (a) Brookes, N. J.; Ariafard, A.; Stranger, R.; Yates, B. F. *J. Am. Chem. Soc.* **2009**, *131*, 5800. (b) Zhao, H.; Lin, Z.; Marder, T. B. *J. Am. Chem. Soc.* **2006**, *128*, 15637. (c) Li, J.; Lin, Z. *Organometallics* **2009**, *28*, 4231.
- (10) Ford, P. C.; Trabuco, E.; Mdleleni, M. M., In *Encyclopedia of Catalysis*, 1st ed; Horváth, I. T., Ed.; Wiley Interscience: Hoboken, NJ, 2003; Vol. 6, pp 651.
- (11) Riduan, S. N.; Zhang, Y.; Ying, J. Y. *Angew. Chem., Int. Ed.* **2009**, *48*, 3322.
- (12) Chakraborty, S.; Zhang, J.; Krause, J. A.; Guan, H. *J. Am. Chem. Soc.* **2010**, *132*, 8872.
- (13) Huang, F.; Lu, G.; Zhao, L.; Li, H.; Wang, Z.-X. *J. Am. Chem. Soc.* **2010**, *132*, 12388.
- (14) (a) Stephens, P. J.; Devlin, F. J.; Chabalowski, C. F.; Frisch, M. J. *J. Phys. Chem.* **1994**, *98*, 11623. (b) Becke, A. D. *J. Chem. Phys.* **1993**, *98*, 5648. (c) Lee, C.; Yang, W.; Parr, R. G. *Phys. Rev. B* **1988**, *37*, 785.
- (15) (a) Wadt, W. R.; Hay, P. J. *J. Chem. Phys.* **1985**, *82*, 284. (b) Hay, P. J.; Wadt, W. R. *J. Chem. Phys.* **1985**, *82*, 270. (c) Hay, P. J.; Wadt, W. R. *J. Chem. Phys.* **1985**, *82*, 299.
- (16) (a) Sang-Aroon, W.; Ruangpornvisuti, V. *Int. J. Quantum Chem.* **2008**, *108*, 1181. (b) Tomasi, J.; Mennucci, B.; Cancès, E. J. *Mol. Struct. Theochem.* **1999**, *464*, 211.
- (17) (a) Carpenter, J. E.; Weinhold, F. *J. Mol. Struct. Theochem.* **1988**, *46*, 41. (b) Reed, A. E.; Weinhold, F. *J. Chem. Phys.* **1983**, *78*, 4066. (c) Foster, J. P.; Weinhold, F. *J. Am. Chem. Soc.* **1980**, *102*, 7211. (d) Glendening, E. D.; Reed, A. E.; Carpenter, J. E.; Weinhold, F. *NBO Version 3.1*.
- (18) Frisch, M. J.; et al. *Gaussian 03, revision E.01*; Gaussian, Inc.: Wallingford, CT, 2004. (See the Supporting Information for the complete reference of Gaussian 03.)
- (19) Schmeier, T. J.; Hazari, N.; Incarvito, C. D.; Raskatov, J. A. *Chem. Commun.* **2011**, *47*, 1824.
- (20) Zhang, J.; Chakraborty, S.; Krause, J. A.; Huang, K.-W.; Guan, H. Unpublished results.
- (21) (a) Zhang, C. G.; Zhang, R.; Wang, Z. X.; Zhou, Z.; Zhang, S. B.; Chen, Z. *Chem.—Eur. J.* **2009**, *15*, 5910. (b) Liang, Y.; Liu, S.; Xia, Y.; Li, Y.; Yu, Z. X. *Chem.—Eur. J.* **2008**, *14*, 4361. (c) Chen, Y.; Ye, S.; Jiao, L.; Liang, Y.; Sinha-Mahapatra, D. K.; Herndon, J. W.; Yu, Z. X. *J. Am. Chem. Soc.* **2007**, *129*, 10773. (d) Yu, Z. X.; Houk, K. N. *J. Am. Chem. Soc.* **2003**, *125*, 13825. (e) Strajbl, M.; Sham, Y. Y.; Villà, J.; Chu, Z. T.; Warshel, A. *J. Phys. Chem. B* **2000**, *104*, 4578. (f) Hermans, J.; Wang, L. *J. Am. Chem. Soc.* **1997**, *119*, 2707. (g) Amzel, L. M. *Proteins* **1997**, *28*, 144.
- (22) (a) Bennaim, A.; Marcus, Y. *J. Chem. Phys.* **1984**, *81*, 2016. (b) Tissandier, M. D.; Cowen, K. A.; Feng, W. Y.; Gundlach, E.; Cohen, M. H.; Earhart, A. D.; Coe, J. V.; Tuttle, T. R. *J. Phys. Chem. A* **1998**, *102*, 7787. (c) Kelly, C. P.; Cramer, C. J.; Truhlar, D. G. *J. Phys. Chem. B* **2006**, *110*, 16066.
- (23) (a) Martin, R. L.; Hay, P. J.; Pratt, L. R. *J. Phys. Chem. A* **1998**, *102*, 3565. (b) Gutowski, K. E.; Dixon, D. A. *J. Phys. Chem. A* **2006**, *110*, 8840. (c) Dinescu, A.; Clark, A. E. *J. Phys. Chem. A* **2008**, *112*, 11198.
- (24) (a) Schlörer, N. E.; Cabrita, E. J.; Berger, S. *Angew. Chem., Int. Ed.* **2002**, *41*, 107. (b) Schlörer, N. E.; Berger, S. *Organometallics* **2001**, *20*, 1703.
- (25) The structures involved in this pathway were optimized at the B3LYP/BSI level. The energies were obtained at B3LYP level with the basis set 6-31+G** for all atoms except Zr (Lanl2DZ basis set). The experimentally employed solvent THF was used to account for solvent effects.
- (26) Zhao, Y.; Truhlar, D. G. *Theor. Chem. Acc.* **2008**, *120*, 215.
- (27) The M06 DFT calculations were performed using Gaussian 09. (See Frisch, M. J.; et al. *Gaussian 09, revision A.01*; Gaussian, Inc.: Wallingford, CT, 2009. See the Supporting Information for the complete reference of Gaussian 09.)
- (28) The reorganization energy was defined as the energy difference between the free PhSiH₃ and the structure similar to the PhSiH₃ moiety in transition states **TSe1** and **TSe2**. Accordingly, the reorganization energies were calculated as 32.6 kcal/mol in **TSe1** and 16.2 kcal/mol in **TSe2**.